machines

MDPI

Article

Analysis of Influential Parameters in the Dynamic Loading and Stability of the Swing Drive in Hydraulic Excavators

Vesna Jovanović [1], Dragoslav Janošević [1], Dragan Marinković [2,3,*], Nikola Petrović [1] and Radomir Djokić [4]

[1] Faculty of Mechanical Engineering, University of Niš, A. Medvedeva 14, 18000 Niš, Serbia; vesna.jovanovic@masfak.ni.ac.rs (V.J.); dragoslav.janosevic@masfak.ni.ac.rs (D.J.); nikola.petrovic@masfak.ni.ac.rs (N.P.)
[2] Department of Structural Analysis, Berlin Institute of Technology, Strasse des 17, Juni 135, 10623 Berlin, Germany
[3] Institute of Mechanical Science, Vilnius Gediminas Technical University, 10105 Vilnius, Lithuania
[4] Faculty of Technical Sciences, University of Novi Sad, Trg Dositeja Obradovića 6, 21000 Novi Sad, Serbia; djokic@uns.ac.rs
* Correspondence: dragan.marinkovic@tu-berlin.de

Abstract: The proper design and configuration of the swing drive mechanism of a hydraulic excavator are crucial to improve energy consumption and efficiency and ensure operational stability. This paper analyzes the influence of the relationship between the parameters of a hydraulic motor and a reducer, which form the integrated transmission of a swing drive, the dynamic characteristics of a hydraulic excavator on loading, and the dynamic stability of the drive. The analysis deals with an excavator model that has the same parameters of the kinematic chain members, the same parameters of the upper structure drive mechanisms, and two variants of the swing drive that, with different integrated transmission parameters, provide the upper structure with the identical number of revolutions and equal rotating moment. One swing drive variant possesses an integrated transmission with a hydraulic motor with a low specific flow and a reducer with a high transmission ratio, while the other drive variant has the opposite parameters. Understanding this relationship is essential for optimizing the design of excavators to achieve better performance and dynamic stability under varying operational conditions. As an example, this paper provides the analysis results regarding the influence of the relationship between the parameters of the integrated transmission hydraulic motor and reducer on the loading and dynamic stability of the swing drive in a tracked hydraulic excavator of 100,000 kg in mass and 4.4 m^3 in loading bucket volume, as obtained from the developed dynamic mathematical models of the excavator using the MSC ADAMS program. The results indicate that the dynamic loads on the swing drive's axial bearing are higher in the variant with a low-specific-flow motor and high transmission ratio reducer during the acceleration and deceleration phases. However, this configuration demonstrated better dynamic stability, with lower oscillation amplitudes and shorter damping times compared to the variant with a high-flow motor and low transmission ratio. Those findings provide valuable criteria for the optimal synthesis of swing drive mechanisms in large hydraulic excavators using multi-criteria optimization methods.

Keywords: hydraulic excavators; swing drive; axial bearing

Citation: Jovanović, V.; Janošević, D.; Marinković, D.; Petrović, N.; Djokić, R. Analysis of Influential Parameters in the Dynamic Loading and Stability of the Swing Drive in Hydraulic Excavators. *Machines* **2024**, *12*, 737. https://doi.org/10.3390/machines12100737

Academic Editor: Piotr Czop

Received: 29 September 2024
Revised: 17 October 2024
Accepted: 18 October 2024
Published: 20 October 2024

1. Introduction

Heavy construction machines are exposed to dynamic loading over the course of their operation, which has a crucial influence on both their stability and lifetime. Their design must adequately account for those dynamic effects in order to avoid premature failure, or even incident failures, as a consequence of instability. Also, the productivity efficiency largely depends on the operator's skill, which cannot provide efficient operation in the long term [1]. For this reason, numerous researchers have dedicated their studies to this important field of work, including the modeling and simulation of the dynamic behavior

of heavy construction machines [2,3], measurements of dynamic loading [4–6], addressing stress states in the load-bearing structures [7–9], identifying stability issues [10–13], and optimization of drive mechanisms [14,15], to name but a few. Among heavy construction machines, hydraulic excavators have the world's largest production with models of various sizes, which are characterized by high-performance engineering, industrial importance, and ergonomic design. An excavator, as a typical multifunctional construction machine, is extensively used in mining excavation, road construction, and large investment projects [16].

In a typical operating cycle for hydraulic excavators, the swing operation accounts for approximately 50–70% of the total working time. During this time, due to the active operation of the swing system drive, energy consumption amounts to 25–40% of the total energy use [17]. In addition, the requirements for the fast acceleration and deceleration of the rotary upper structure during the swing operation cause frequent switching of the acceleration and deceleration of the motor, which leads to higher energy consumption and reduced efficiency, as well as to a state of excessive or insufficient matching with the required function parameters [18]. To improve the energy efficiency and dynamics of the swing system, Lijie Zhang et al. [17] suggest adding two pressure-reducing valves (PRVs) to the main valve pilot control circuit of excavators, along with a pump-valve compound control strategy. The simulation results demonstrate that this approach reduces motor overflow, improves braking stability, and enhances the swing system's response during operations. In Ref. [19], an adaptive sliding mode controller with a nonlinear extended state observer that realizes position-tracking of the swing upper structure is proposed. This controller employs current deviations, added to error signals, to ensure torque balance. In this way, the work performance and energy efficiency of the electro-mechanical swing system are improved; these systems are widely used in medium-sized excavators. In Ref. [20], a new design for the swing drive's hydraulic motor in hydraulic excavators is proposed, with the aim of analyzing the impact of hydraulic motor parameters on the energy efficiency of the drive. The dual-source hydraulic motor integrates an energy recovery unit and the main drive unit, forming two separate hydraulic flows to avoid energy loss during braking, as is common in conventional swing drives. The displacement ratio in the context of the dual-source hydraulic motor is defined as the ratio between the displacements of two different oil circuits in the motor. The displacement ratio is a critical factor because it influences the performance characteristics of the hydraulic motor and the overall system. The key findings include a significant reduction in energy consumption by the hydraulic pump in the main drive unit when using the dual-source system compared to the original system.

However, in conventional swing drive systems, the production efficiency and positioning accuracy of the excavator manipulator during rotation depend on the operator's reaction speed. To overcome this issue, Ref. [21] proposes a combined position and speed control strategy without changing the conventional operating method, using the desired position or rotation angle as the input signal for the closed-loop position control. Additionally, to improve the dynamic characteristics of the swing drive during braking, the principle of energy balance is used by varying the valve's opening size during the swing process.

Incorrect design or modification of the existing design can lead to poor results, including increased vibration levels and other electronic or mechanical issues. Additionally, the cost of upgrading hydraulic systems is a limiting factor for instituting changes. The wide availability of integrated transmissions in excavator design offers the possibility of synthesizing various swing drive options with lower specific hydraulic motor flow and higher gear ratios, or vice versa. Therefore, as a contribution to improving the dynamic characteristics of conventional swing drives, which are the most common drives in large hydraulic excavators, this paper analyzes the impact of the ratio of the hydraulic motor and reducer parameters of integrated transmission on the stability and efficiency of the drive, based on the proposed dynamic mathematical model of the excavator. The analysis

results can, thus, become one of the most influential criteria, with a high significance factor, in the optimal selection of drives using one of the multi-criteria optimization methods.

Hydraulic excavators of all sizes equipped with various tools perform numerous functions using spatial manipulation (Figure 1a). The kinematic chain of an excavator consists of an undercarriage with tracks L_1 and upper structure L_2, which has a cabin, boom L_3, stick L_4, and bucket L_5. In the kinematic chain of an excavator, spatial manipulation is enabled by the rotary upper structure L_2, which is connected with the undercarriage using a slewing joint in the form of an axial bearing. The general design of the hydrostatic drive of the rotary upper structure comprises a hydraulic pump (2.1, Figure 1b) driven by a diesel engine (1), hydraulic motor (2.3), reducer (2.4), and axial bearing (2.5). It is characteristic that the hydraulic motor and the reducer form an integrated transmission, where the separate modules are produced by specialized manufacturers, with very different parameters for all sizes of excavators and other mobile machines. The process of selecting the swing drive components begins with choosing the size of the axial bearing, based on the load. Previous research mainly focuses on: (a) the loading of large-diameter axial bearings [22–25], (b) the loading of the track for rolling elements in axial bearings [26–28], (c) studies into the influential factors for determining bearing load capacity in diagrams, used as the basis for the selection of axial bearings, in comparison with equivalent loads [29–32], and (d) the loading of the screw joints of axial bearings [33–36].

Modern design procedures have conditioned the development of certain modules of drive and control systems in mobile machines. Among the developed modules is one for the integrated transmission (hydraulic motor—reducer) of swing drives in hydraulic excavators of all sizes [37]. The developed modules are characterized by the ability to design the same model of an integrated transmission of a rotary upper structure with a determined output moment by using several hydraulic motors with different specific flows and several reducers with different transmission ratios.

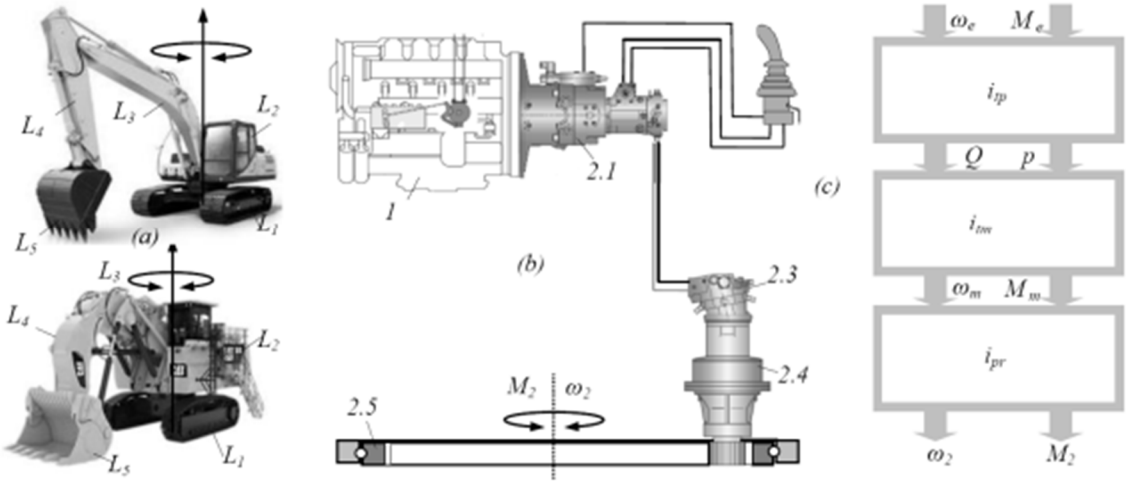

Figure 1. The general design of the swing drive mechanism in hydraulic excavators: (**a**) physical excavator models [38], (**b**) functional drive schematic, (**c**) drive block.

When synthesizing the swing drive mechanism in line with the given output upper structure parameters, it is necessary to select an optimal solution from a set of possible variant solutions for an integrated drive transmission using the appropriate transformation and transmission parameters, thereby developing a hydraulic motor with a particular specific flow and a reducer with a particular transmission ratio.

This paper presents the results of an analysis of the relationship between the integrated transmission hydraulic motor and reducer parameters, i.e., the relationship between the specific flow of the hydraulic motor and the transmission ratio of the reducer forming the integrated transmission in terms of the loading and dynamic stability of the swing drive in hydraulic excavators.

First, the transmission functions were established; these relate to the input and output parameters of the swing drive. After that, two mathematical models of the excavator with rigid and elastic bodies were developed to determine the drive load, based on which the transmission and transformation parameters of the integral drive were selected. Then, two variants of drives with extreme values were separated, using the same parameters of the swing drive function, in order to analyze the influence of different parameters on the stability of the excavator.

2. Swing Drive Parameters

In principle, the general model of the drive mechanism of a swing drive in hydraulic excavators possesses a hydrostatic-mechanical design, with transformation and transmission parts. In the transformation part, the angular velocity ω_e, shown in Figure 1c, and moment M_e of the diesel engine 1, shown in Figure 1b, are transformed by the hydraulic pump 2.1 into hydraulic power parameters—pressure p and flow Q, which, in turn, are transformed by the hydraulic motor 2.3 into the mechanical power parameters—angular velocity ω_m and moment M_m. In the transmission–mechanical part, the hydraulic motor angular velocity and moment are further transformed, using the reducer 2.4 and axial bearing 2.5, into the desired angular velocity ω_2, i.e., the number of revolutions n_2 and moment M_2 of the rotary upper structure. The input and output parameters of the swing drive are connected by the following transmission functions:

- For the number of rotary upper structure revolutions:

$$n_2 = \frac{q_{pmax} \cdot \varepsilon_p \cdot n_p}{q_{mmax} \cdot \varepsilon_m} \cdot \eta_{pv} \cdot \eta_{mv} \cdot \frac{1}{i_r \cdot i_l}\ , \tag{1}$$

- For the rotary upper structure drive moment:

$$M_2 = \frac{(p - p_o) q_{mmax} \cdot \varepsilon_m}{2\pi} \cdot \eta_{mm} \cdot i_r \cdot \eta_r \cdot i_l \cdot \eta_l\ , \tag{2}$$

where: q_{pmax}, q_{mmax}—the maximum specific flow of the hydraulic pump and the hydraulic motor, p, p_o—the pressure in the extension and retraction duct of the hydraulic motor, n_p—the number of the hydraulic pump revolutions, i_r, η_r—the transmission ratio and the degree of efficiency of the reducer, η_{pv}, η_{pm}, η_{mv}, η_{mm}—the volumetric and mechanical degrees of efficiency of the hydraulic pump and the hydraulic motor, $\varepsilon_p = q_p / q_{pmax}$—the hydraulic pump regulation range, $\varepsilon_m = q_m / q_{mmax}$—the hydraulic motor regulation range, and η_l—the degree of efficiency between the reducer and the axial bearing. The above transmission functions show that the same output parameters of the swing drive, the number of revolutions n_2, and moment M_2 can be achieved with a lower specific flow of the hydraulic motor q_m and a higher transmission ratio i_r of the reducer (and vice versa) for the selected axial bearing and given pressure p, specific flow q_p, and number of revolutions n_p of the hydraulic pump.

Dynamic Mathematical Models of the Excavator

To analyze the influence of the relationship between the sizes of the integrated transmission hydraulic motor and the reducer of the swing drive on the excavator's loading and dynamic stability, two dynamic mathematical models for the hydraulic excavator were developed. The models encompass the general configuration, which incorporates an undercarriage with tracks L_1 and a upper structure with a cabin L_2, boom L_3, stick L_4, bucket with a support plate L_5, and jaws L_6 (Figure 2). The first dynamic mathematical model of the excavator assumes rigid members for the undercarriage and upper structure (Figure 2b).

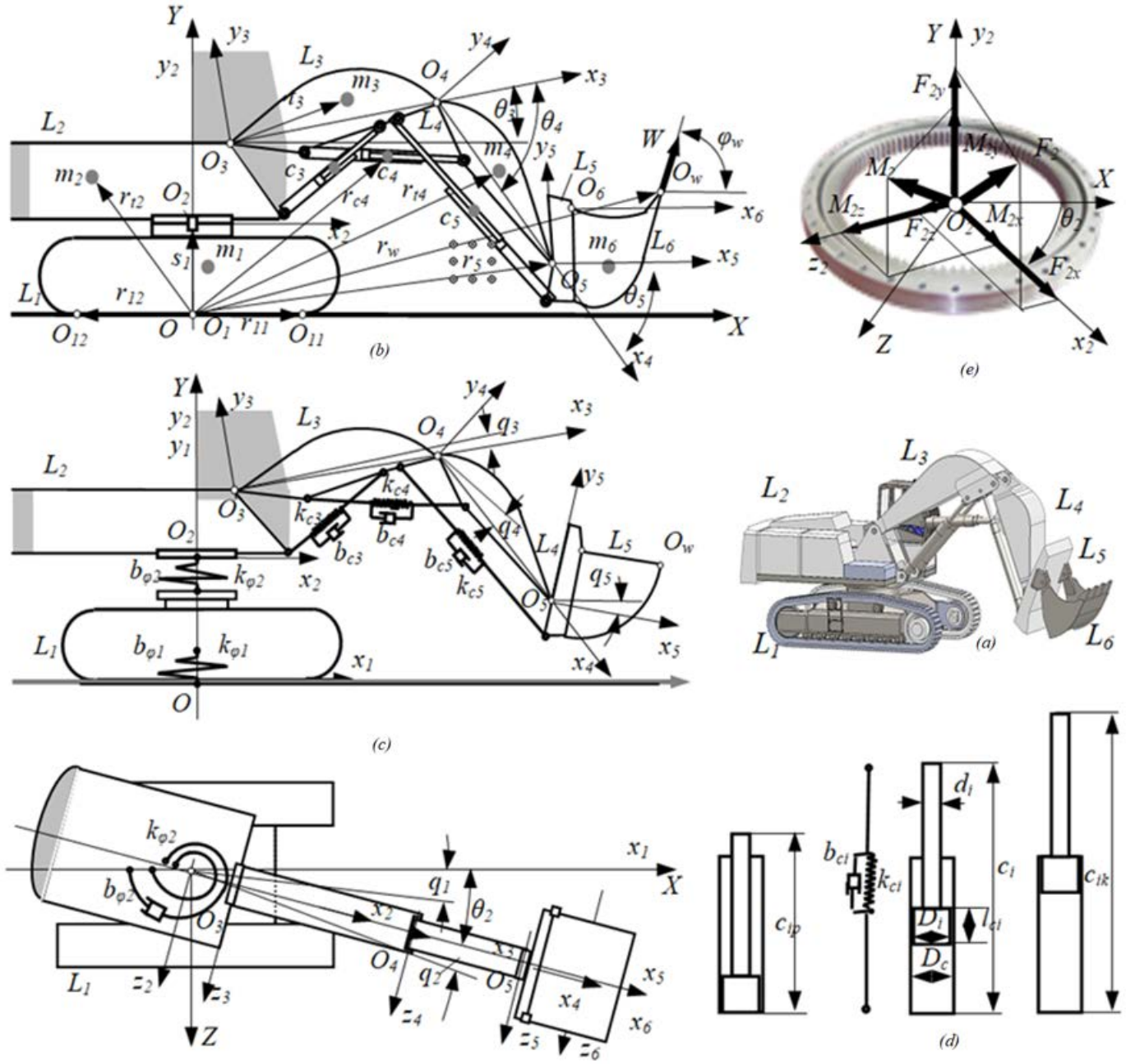

Figure 2. Models of excavators with a loading manipulator: (**a**) physical model, (**b**) rigid dynamic model, (**c**) elastic dynamic model, (**d**) elastic-damping characteristics of the manipulator's hydraulic cylinder, (**e**) loading force and moment components for joint O_2 of the kinematic pair comprising the undercarriage and upper structure.

The ground is also modeled like a rigid body. During the manipulation task, the excavator is subjected to external (technological) load—digging resistance force and the digging resistance moment (during the digging operation), along with internal load—the force of gravity (weight) and the inertia forces and moments of each member, hydraulic cylinders, and material scooped by the excavator bucket. The boom, arm, and bucket hydraulic cylinders are modeled as rods with equally distributed mass along the current length. In the joints of the excavator, friction is neglected, as is the influence of wind on the members.

The space of the excavator model is determined using an absolute coordinate system *OXYZ*, shown in Figure 2b, with the unit vectors *i*, *j*, and *k* in the direction and

sense of the coordinate axes OX, OY, and OZ. The excavator undercarriage lies in the horizontal plane OXZ of the absolute coordinate system, while the vertical axis OY of the same system corresponds to the axis of the kinematic pair of the undercarriage and upper structure. Every member of the excavator kinematic chain L_i and each hydraulic cylinder are completely determined in their local coordinate system, $O_i\ x_i\ y_i\ z_i$, by a set of required parameters [29]. In the mathematical model of the excavator, the position of the kinematic chain members is determined using the following generalized coordinates, as shown in Figure 2b: θ_1—the displacement of the undercarriage in the horizontal plane, θ_2—the angle of the upper structure's position, θ_3, θ_4, θ_5, θ_6—the angles of the relative positions of the boom, stick, and bucket support plate and jaws of the excavator. The swing drive mechanism c_2 is determined using the following quantities: q_{2max}/q_{2min}—the maximum/minimum specific flow of the hydraulic motor, i_r—the transmission ratio of the integrated transmission reducer, i_l—the transmission ratio between the gear on the output shaft of the reducer and the toothed ring of the axial bearing, and n_{c2} and m_{c2}—the number and the mass of the swing drives. The second, elastic, dynamic mathematical model of the excavator Figure 2c involves the members of the undercarriage and upper structure, which have elastic-damping characteristics. The ground also possesses elastic-damping characteristics. The boom, stick, and bucket's hydraulic cylinders and the hydraulic motors of the swing drive mechanism possess elastic-damping characteristics that occur due to the compressibility of hydraulic oil in the operating capacities and hydraulic ducts of the actuators. The modulus of compressibility of hydraulic oil is constant and does not depend on pressure and temperature.

The elastic dynamic characteristic of the hydraulic motor of the swing drive's integrated drive transmission is the hydraulic torsional rigidity k_{h2}, which is defined by the following equation [39]:

$$k_{h2} = \frac{2 \cdot \left(\frac{q_{2m}}{2\pi}\right)^2 \cdot E_o}{\frac{q_{2m}}{2} + \frac{d_{vm}^2 \cdot \pi}{4} \cdot l_{vm}}, \tag{3}$$

where: q_{2m}—the specific flow of the hydraulic motor, E_o—the modulus of elasticity (compressibility) of hydraulic oil, and d_{vm}, l_{vm}—the internal diameter and length of the operating ducts of the hydraulic motor, from the hydraulic motor to the distribution valves that, in modern drives, are directly linked to the hydraulic motor in the open and closed hydrostatic circuit.

The torsional rigidity of the swing drive is determined by reducing the hydraulic torsional rigidity of the hydro motor:

$$k_{\varphi 2} = k_{h2} \cdot i_r^2 \cdot i_l^2, \tag{4}$$

where: i_r, i_l—the transmission ratio of the integrated transmission reducer and the transmission ratio between the output shaft of the reducer and the toothed bearing ring of the excavator's swing drive mechanism.

Due to the compressibility of hydraulic oil, the hydraulic cylinders of the excavator are modeled using hydraulic springs with appropriate rigidity (Figure 2d):

$$k_{ci} = \frac{\left(\frac{D_i^2 \cdot \pi}{4}\right)^2 \cdot E_o}{\frac{D_i^2 \cdot \pi}{4}\left(c_i - c_{ip}\right) + \frac{d_{vi}^2 \cdot \pi}{4} \cdot l_{vi}} + \frac{\left(\frac{D_i^2 - d_i^2}{4} \cdot \pi\right)^2 \cdot E_o}{\frac{D_i^2 - d_i^2}{4} \cdot \pi \cdot \left(c_{ik} - c_i\right) + \frac{d_{vi}^2 \cdot \pi}{4} \cdot l_{vi}} \quad \forall i = 3, 4, 5, \tag{5}$$

where: D_i, d_i—the diameter of the piston and the piston rod in the hydraulic cylinders, c_{ip}, c_i, c_{ik}—the initial, current, and final length of the hydraulic cylinders, and d_{vi}, l_{vi}—the internal diameter and length of the operation ducts of the hydraulic cylinders, from the hydraulic cylinders to the distribution valves of the excavator drive system.

The damping coefficients of the hydraulic cylinders, according to Figure 2e, are determined using the following expression [39]:

$$b_{ci} = \frac{\pi \cdot \eta_o \cdot l_{ci} \cdot D_i^2}{(D_{ci} - D_i)^2} \left[3 + \frac{3}{4} \frac{d_{i1}}{(D_{ci} - D_i)} \right] \quad \forall i = 3, 4, 5 \tag{6}$$

where: η_o—the dynamic viscosity of hydraulic oil, l_{ci}—the length of the hydraulic cylinder piston, and D_{ci}—the internal diameter of the hydraulic cylinder.

3. Dynamic Loading of the Swing Drive

The following analysis of the influence of the relationship between the hydraulic motor and the reducer, which form the integrated transmission of the swing drive, on the loading of the drive mechanism is based on loading values in the center of joint O_2 in the kinematic pair comprising the undercarriage and upper structure. Joint O_2's center loads are determined by a numerical simulation of the excavator, based on the defined rigid and elastic dynamic mathematical model of the excavator. The center of joint O_2 in the undercarriage–upper structure kinematic pair is the point of intersection of the vertical joint axis O_2y_2 and the horizontal plane in which the centers of the rolling elements of the axial bearing of the swing drive are positioned.

By fictively breaking the excavator kinematic chain in the center of joint O_2, and by observing the balance of the part of the chain that is formed by the cabin and the manipulator, the vectors of force F_2 and moment M_2 of joint O_2 loading can be determined, as shown in Figure 2e:

$$F_2 = \sum_{i=2}^{6} F_{ui} + \sum_{i=3}^{6} F_{cui} + W \,, \tag{7}$$

$$M_2 = \sum_{i=2}^{6} M_i + \sum_{i=3}^{6} M_{ci} + \sum_{i=2}^{6} M_{Fui} + \sum_{i=3}^{6} M_{Fcui} + M_w \,, \tag{8}$$

where: F_{ui}, M_i,—the internal force (inertia and gravity) and the inertia moments in the center of the mass of the excavator kinematic chain member, M_{Fui}—the moment of the internal force of the excavator kinematic chain member for the center of joint O_2, F_{cui}, M_{ci},—the internal force (inertia and gravity) and the inertia moments in the center of the mass of the actuator (hydraulic cylinder), M_{Fcui}—the moment of the internal force of the drive mechanism actuators for the center of the joint O_2 axis, W—the digging resistance force, and M_w—the moment of the digging resistance force for the center of the joint O_2 axis.

As an example, working on the basis of the defined mathematical models of the excavator and using the procedure for dynamic numerical simulation in the ADAMS software 2020, the vectors of force F_2 and moment M_2 of the center of joint O_2 were determined for a tracked excavator of m = 100,000 kg in mass and V = 4.4 m^3 in terms of loading bucket volume for the different variants A and B of the swing drive. These swing drives possess the same axial bearings and different integrated transmissions in terms of the size of the specific flow of the hydraulic motor and the transmission ratio of the reducer. Drive variant A, with an integrated transmission drive, has a hydraulic motor with a specific flow of $q_{m2}a$ = 80.4 cm^3 and a reducer with a transmission ratio of i_{ra} = 111.86, while drive variant B with integrated transmission has a hydraulic motor with a specific flow of q_{m2b} = 200 cm^3 and a reducer with a transmission ratio of i_{ra} = 35.13.

The adopted different variants, A and B, of the swing drive were selected out of a set of 21 possible variant solutions as yielding the extreme values of a specific flow-transmission ratio, as determined through a synthesis procedure based on the maximum given number of revolutions of n_2 = 5 min^{-1} and a moment of rotation of M_2 = 500 kNm, calculated for the upper structure of an excavator model with a mass of m = 100,000 kg. The drive synthesis calculations employed a database of the available models of swing drive integrated transmissions manufactured by Bosch Rexroth [37].

For the adopted excavator model in this analysis of swing drive loading, the following input values were fed into the program: the parameters of the excavator's kinematic chain members, determined in line with the developed 3D excavator model, shown in Figure 2d, the rigidities and damping coefficients of the support surface of the undercarriage, listed in Table 1, the rigidities and damping coefficients of the excavator's swing drive, determined on the basis of the parameters of the drive variants *A* and *B* listed in Table 2, the rigidities and damping coefficients of the hydraulic cylinders of the boom, stick, and bucket, determined according to the parameters of the manipulator drive mechanisms in Table 3, as well as the conditions of dynamic numerical simulations pertinent to the parameters of the excavator manipulation task as given in Figure 3.

Table 1. Dynamic characteristics of the undercarriage and the excavator's support surface.

Parameter	Symbol	Dimension	Value
Torsional rigidity of the support surface and undercarriage	$k_{\varphi 1}$	Nm/rad	7.056×10^9
Torsional damping of the support surface and undercarriage	$b_{\varphi 1}$	Nms/rad	7.056×10^7

Table 2. Dynamic characteristics of the variant solutions of the swing mechanism transmission.

Parameter	Symbol	Dimension	Transmission Variants	
			VB50/2	VB87/2
Specific flow of the hydraulic motor	q_{2m}	cm^3	80.40	200.00
Internal diameter of the hydraulic motor ducts	d_{vm}	m	0.025	0.032
Length of the hydraulic motor ducts	l_{vm}	m	0.320	0.320
Hydraulic rigidity of the hydraulic motor	k_{h2}	Nm/rad	2327	7949
Damping coefficient of the swing drive	b_{c2}	s^{-1}	0.879	0.879
Oil modulus of elasticity	E_o	N/m^2	1.4×10^9	1.4×10^9
Reducer transmission ratio	i_r	-	111.86	35.13
Transmission ratio between the reducer shaft and the bearing	i_l	-	6.93	6.93

For the purposes of this analysis, the conditions of the dynamic numerical simulation of the excavator are derived from the change in the angular velocities (Figure 3) of the relative movement of the excavator kinematic chain members during the manipulation task, which includes the following operations: scooping the material and loading it into the bucket, transferring and unloading the material, and returning to a position that is ready for a new scooping operation.

During the operation of scooping the material with the loading bucket, a modeled change in the resistance force vector *W* is given, with the force acting on the cutting edge of the bucket during digging and scooping material of γ = 1800 kg/m^3 in density. From the results of the swing drive loading analysis, obtained using the ADAMS program, and based on the elastic dynamic mathematical model of the excavator, wherein the excavator support surface and drive mechanism actuators are modeled as elastic-damping elements, the changes in the components of the joint O_2 loading force F_{2xe}, F_{2ye}, $F_{2ze,}$ shown in Figure 4, and moment M_{2xe}, M_{2ye}, M_{2ze}, shown in Figure 5, are extracted with regard to the duration of the excavator manipulation task. In addition, for the sake of comparison, the changes in the components of the joint O_2 loading force F_{2xk}, F_{2yk}, F_{2zk}, shown in Figure 4, and moment M_{2xk}, M_{2yk}, M_{2zk}, shown in Figure 5, are also given, these having been obtained by

a dynamic numerical simulation based on the rigid mathematical model of the excavator, in which the excavator support surface, kinematic chain members, and drive mechanism actuators are modeled using rigid bodies.

Table 3. Dynamic characteristics of the excavator manipulator mechanism.

Parameter	Symbol	Dimension	Hydraulic Cylinders		
			Boom	Stick	Bucket
Diameter of the hydraulic cylinder piston	D_i	m	0.280	0.250	0.220
Diameter of the hydraulic cylinder piston rod	d_i	m	0.200	0.180	0.160
Internal diameter of the hydraulic cylinder	d_{ci}	m	0.2805	0.2505	0.2205
Initial length of the hydraulic cylinder	c_{ip}	m	2.800	2.300	3.150
Final length of the hydraulic cylinder	c_{ik}	m	4.500	3.500	4.100
Number of hydraulic cylinders	n_{ci}	-	2	2	2
Internal diameter of the hydraulic cylinder ducts	d_{vi}	m	0.048	0.048	0.048
Length of the hydraulic cylinder ducts	l_{vi}	m	6.000	6.000	7.000
Dynamic viscosity of hydraulic oil	η_o	Ns/m^2	0.09	0.09	0.09

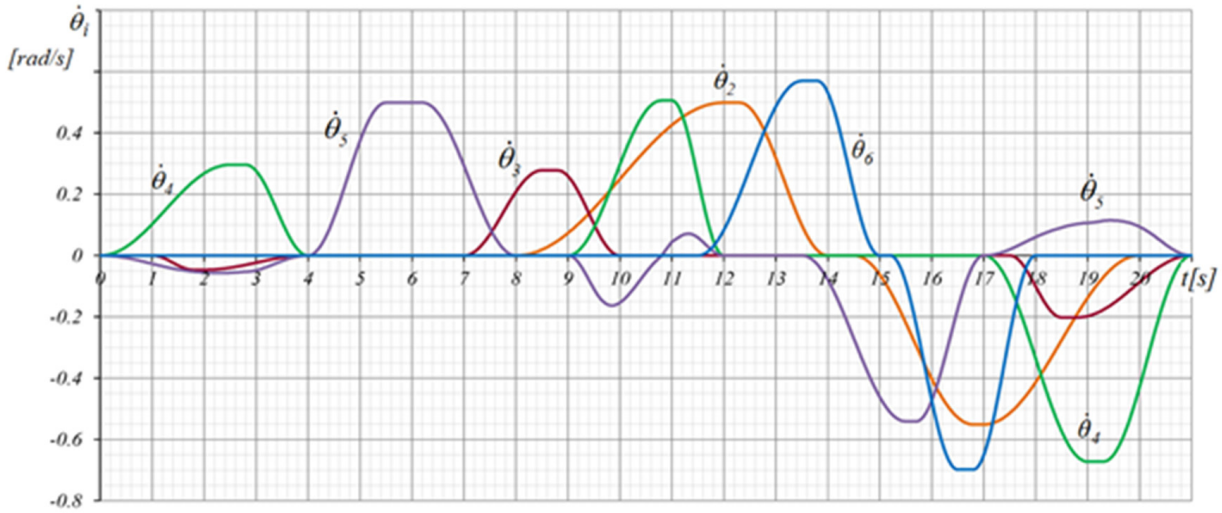

Figure 3. Change in the angular velocities of the relative movement of the excavator kinematic chain members: $\dot{\theta}_2$—upper structure with $\dot{\theta}_3$—boom, $\dot{\theta}_4$—stick, $\dot{\theta}_5$—bucket support, and $\dot{\theta}_6$—jaws.

The comparative analysis shows that during the digging operation, when the swing drive is not active, there is no significant difference in the changes in the force vector components F_{2xk}, F_{2yk}, F_{2zk}, shown in Figure 4, and the moment vector components M_{2xk}, M_{2yk}, M_{2zk}, shown in Figure 5, previously obtained using the rigid model of the excavator in comparison with the force components F_{2xe}, F_{2ye}, F_{2ze} and moment components M_{2xe}, M_{2ye}, M_{2ze}, obtained using the elastic model of the excavator. In addition, during the digging operation, there are no significant changes in the value of joint O_2 loading between swing drive variants *A* and *B*. The differences in the joint O_2 loading are observed only during the transferring operation and while the excavator is returning to a new digging plane when the swing drive is active.

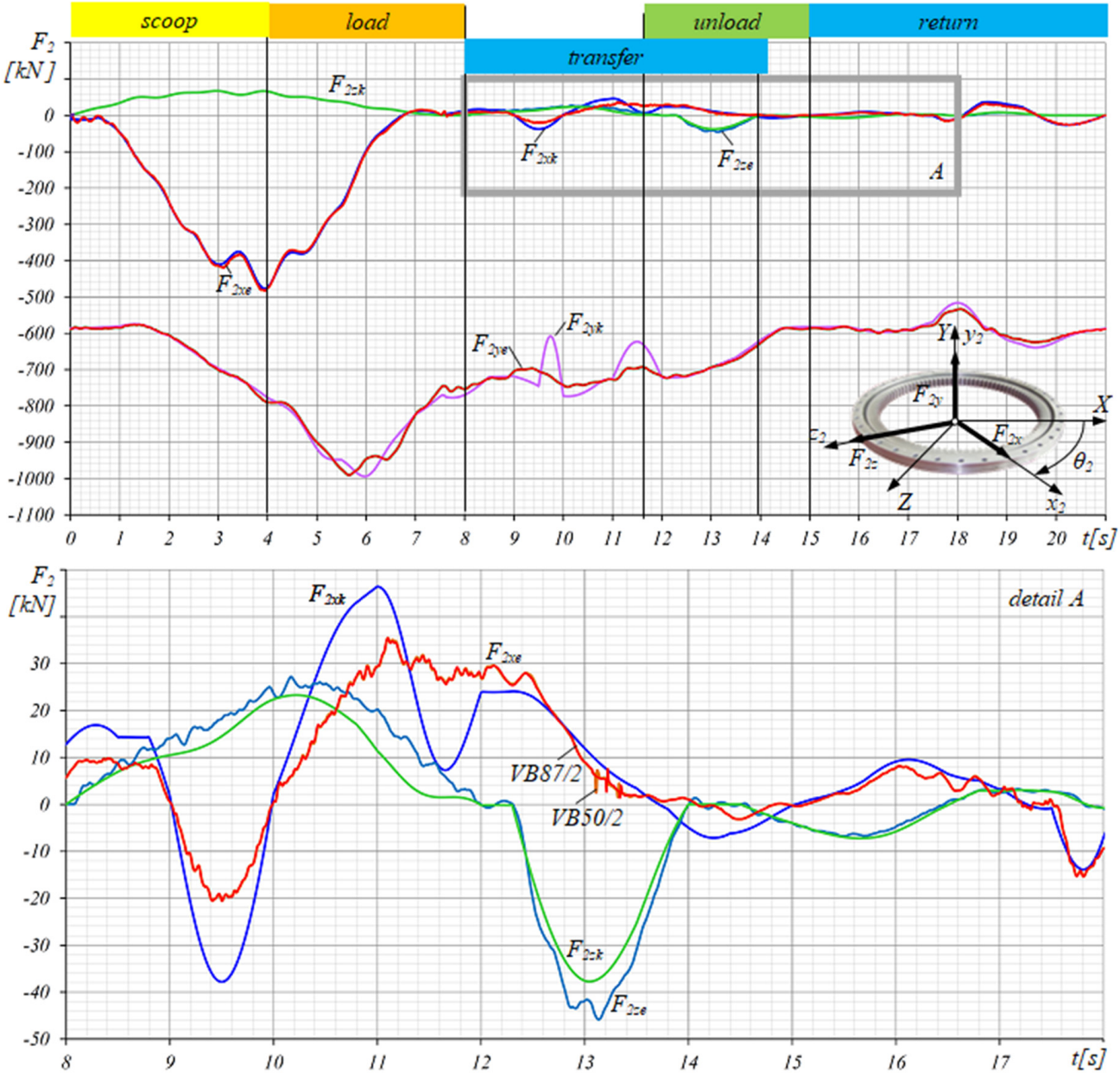

Figure 4. Components of joint O_2 loading forces for the swing drive variants *A* and *B*, determined with the rigid (F_{2xk}, F_{2yk}, F_{2zk}) and the elastic (F_{2xe}, F_{2ye}, F_{2ze}) mathematical models of the excavator.

During the digging and scooping operations (t = 8 s), joint O_2 loading does not differ for drive variants *A* and *B*. The zoomed change in the joint O_2 loading during the excavator manipulation task (t = 8–18 s), as given in Figure 4, shows a slight difference in the changes in the force components F_{2xk} and F_{3xe} in the initial period (t = 9.5–12.5 s) of the accelerated rotation of the upper structure during the material transfer operation. In the same period, the change in force F_{2xe} is identical with variants *A* and *B*. Insignificant oscillatory changes in force F_{2xe} appear with the change between swing drive variants *A* and *B* (t = 13.5 s) at the beginning of the decelerating (stopping) rotation. Here, somewhat greater amplitudes appear in the changes in force F_{2xe} intensity with the drive variant *A*, the integrated transmission of which has a lower specific flow for the hydraulic motor (q_{m2a} = 80.4 cm^3) and a higher transmission ratio for the reducer (i_{ra} = 111.86).

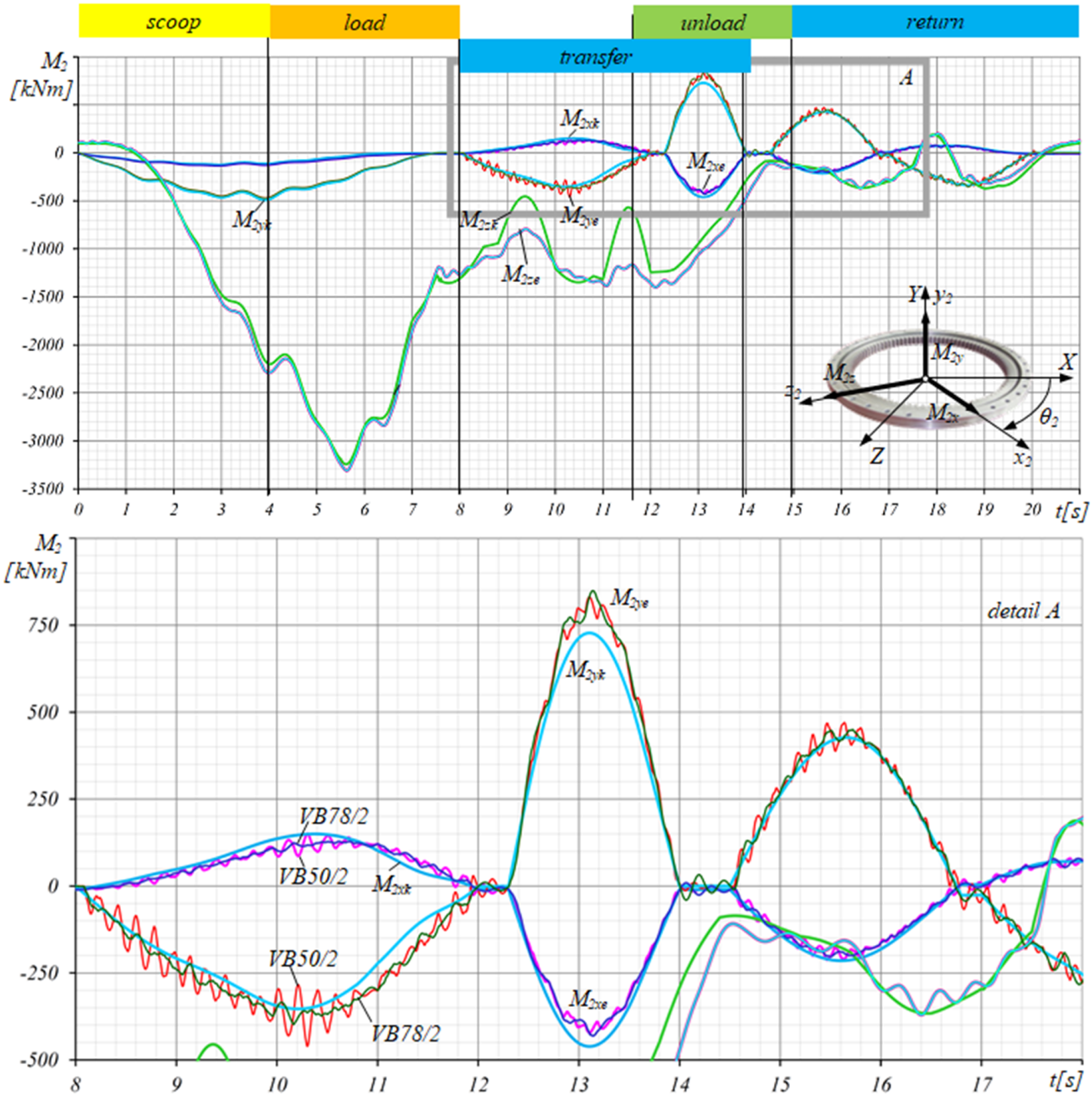

Figure 5. Components of joint O_2 loading moments for the swing drive variants *A* and *B*, determined with the rigid (M_{2xk}, M_{2yk}, M_{2zk}) and the elastic (M_{2xe}, M_{2ye}, M_{2ze}) mathematical models of the excavator.

Components F_{2yk} and F_{2ye} of the joint O_2 loading force vector do not change significantly during the manipulation task. Smaller deviations in the intensity (t = 10–12 s) appear at the end of the accelerated upper structure rotation. Components F_{2zk} and F_{2ze} of the joint O_2 loading force vector differ insignificantly in terms of change intensity and character during the manipulation task. The change in components F_{2ze} and F_{2ze} of the joint O_2 loading force is the same for both variants *A* and *B* of the excavator swing drive. The zoomed-in part of the changes in the joint O_2 loading moment components, depicted in Figure 5, shows that during the material transfer operation (t = 9–13 s) when the swing drive mechanism is active, the character of the oscillatory changes in components M_{2xe} and M_{2ye} is not the same for drive variants *A* and *B*. Here, greater amplitudes appeared

during the changes in intensity with drive A, particularly in moment component M_{2ye} at the beginning of the accelerated rotation (t = 9–10.5 s). In the same stage of the manipulation task, a difference appears in the intensity of changes in components M_{2zk} and M_{2ze}, which is determined based on the rigid and elastic mathematical models of the excavator.

4. Dynamic Stability of the Swing Drive

The basis for this analysis of the influence of the relationship between the parameters of the hydraulic motor and the reducer that form the integrated transmission of the excavator swing drive on the dynamic stability drive is represented by the previously defined elastic dynamic excavator model, with five degrees of freedom of movement determined by the following generalized oscillation coordinates, as shown in Figure 2b:

$$q = \{q_1, q_2, q_3, q_4, q_5\}\ , \tag{9}$$

where: q_1—the turning angle of the undercarriage in the horizontal plane around its vertical axis O_1y_1, q_2—the turning angle of the upper structure around its vertical axis O_2y_2, and q_3, q_4, q_5—the turning angles of the boom, stick, and bucket around the horizontal axes O_iz_i of the swing joints by which they are connected to the kinematic chain of the excavator manipulator.

In the excavator model, as a single member of the manipulator, the bucket comprises the connected bucket support plate and jaws, along with the hydraulic cylinders for the movement of the jaws.

This analysis highlighted small oscillations of the excavator kinematic chain members around the position of stable balance, due to the elastic-damping characteristics of the actuators (hydraulic motors and hydraulic cylinders) of the excavator drive mechanisms caused by the initial movement conditions. Based on the defined mathematical model, and using the ADAMS program as an example, generalized oscillation coordinates were determined for the already adopted excavator model of 100,000 kg in mass with the swing drive variants A and B. The initial movement conditions, listed in Table 4, correspond to the position of the excavator kinematic chain in the initial decelerated phase of the operation of returning the upper structure (t = 16.76 s), shown in Figure 3, from the unloading plane to the new plane of digging via a sharp decrease in the initial angular velocity of the upper structure from $\dot{\theta}_2 = -0.551$ rad/s to $\dot{\theta}_2 = 0$ rad/s. From the obtained analysis results, we present the change in the generalized oscillation coordinate q_2, as depicted in Figure 6, of the upper structure for the drive variants A and B, which shows that the relationship between the parameters of the drive integrated transmission influences its dynamic stability.

Table 4. Initial excavator oscillation conditions.

Parameters of Initial Conditions	Symbol	Dimension	Values
Manipulation task time	t	s	16.76
Undercarriage position angle	θ_1	°	0.000
Upper structure angle	θ_2	°	54.342
Boom position angle	θ_3	°	50.526
Stick position angle	θ_4	°	−42.292
Bucket position angle	θ_5	°	−37.282
Upper structure angular velocity	$\dot{\theta}_2$	rad/s	−0.551

The oscillation of the excavator with the variant A drive, the integrated transmission of which has a hydraulic motor with a lower specific flow (q_{m2a} = 80.4 cm^3) and a reducer with a higher transmission ratio (i_{ra} = 111.86), yields significantly lower amplitudes and periods of damped oscillations in relation to the variant B drive, which has an integrated transmission including a hydraulic motor with a higher specific flow (q_{m2b} = 200 cm^3) and a reducer with a lower transmission ratio (i_{ra} = 35.13) for the same initial conditions of the excavator's movement. Furthermore, the time needed for the oscillation of the upper

structure with the variant A drive to subside (t_{sa} = 1.5 s) is significantly shorter than the time needed for the oscillation of the upper structure with the variant B drive to subside (t_{sb} = 3 s).

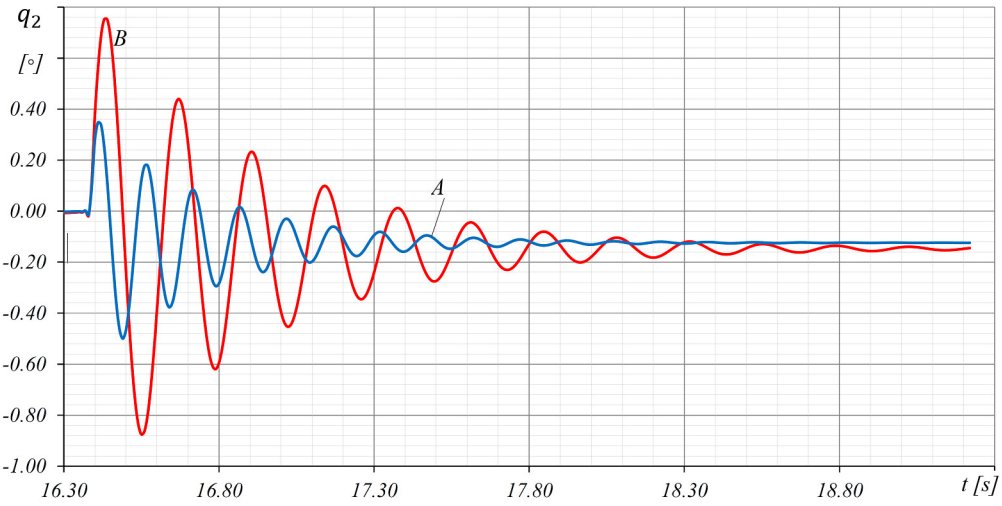

Figure 6. Generalized oscillation coordinates of the excavator upper structure with drive variants *A* and *B*.

5. Conclusions

The results of the analysis presented in the paper show that the dynamic loading and dynamic stability of the swing drive mechanism in hydraulic excavators depend on the relationship between the parameters of the hydraulic motor and the reducer comprising the integrated transmission of the swing drive. The relation of the parameters represents the relation between the magnitude of the specific flow of the hydraulic motor and the transmission ratio of the reducer in the integrated transmission, bearing in mind that the same number of revolutions and the upper structure rotation moment can be achieved using a hydraulic motor with a low specific flow and a reducer with a high transmission ratio, and vice versa.

For this analysis of the loading of the swing drive mechanism, the force and moment vectors of the center of the drive axial bearing were determined using the procedure of numerical simulation employed for the operation of an excavator weighing 100,000 kg, in line with the given conditions of the manipulation task and with the following operations: scooping, transferring, and unloading the material and returning to the new digging position. The obtained results show that the dynamic loads of the drive axial bearing are larger in a swing drive with an integrated transmission that has a hydraulic motor with a lower specific flow and a reducer with a higher transmission ratio, compared to an integrated transmission that has a hydraulic motor with a higher specific flow and a reducer with a lower transmission ratio. The difference in the axial bearing loads is particularly pronounced in the phases of accelerated and decelerated movement of the upper structure during the operation of transferring the scooped material.

For this analysis of the dynamic stability of the swing drive, a dynamic mathematical model was developed in which the chain members were modeled using rigid bodies, while the actuators (hydraulic motors and hydraulic cylinders) of the excavator drive mechanisms were modeled as elastic-damping elements. Small oscillations were observed in the kinematic chain members around the balance position for the given initial conditions of the upper structure movement. The analyses showed that when the swing drive with an integrated transmission, a hydraulic motor with a lower specific flow, and a reducer with a higher transmission ratio was compared with the drive that had an integrated transmission with the opposite parameters, the first swing drive displayed significantly lower oscillation

amplitudes and a shorter time for damping the oscillation of the upper structure under the same initial movement conditions.

The obtained research results, as presented in this paper, can contribute to future research related to the development of a multi-criteria method for selecting the best drive solution for excavators. A multi-criteria analysis with economic and technical indicators [40] is necessary to evaluate the generated variants of the platform drive solution. Additionally, future studies can focus on applying advanced optimization algorithms, such as machine learning-based methods, to improve the balance between hydraulic motor flow and transmission ratios, thereby enhancing both energy efficiency and dynamic stability under diverse operating conditions.

Author Contributions: Conceptualization, V.J. and D.J.; methodology, D.J.; software, V.J.; validation, V.J., D.J. and D.M.; formal analysis, V.J.; investigation, V.J.; resources, N.P.; data curation, V.J.; writing—original draft preparation, V.J.; writing—review and editing, D.J. and D.M.; visualization, R.D.; supervision, D.M.; funding acquisition, D.M. All authors have read and agreed to the published version of the manuscript.

Funding: This research was financially supported by the Ministry of Education, Science and Technological Development of the Republic of Serbia (Contract No. 451-03-9/2021-14/200109).

Data Availability Statement: Data are contained within the article.

Conflicts of Interest: The authors declare no conflicts of interest.

References

1. Geralda, L.N.; Muhammad, A.; Himmawan, S.A.; Diky, Z. Performance Improvement of Hydraulic Excavator Efficiency. *J. Mechatron. Artif. Intell.* **2024**, *1*, 27–44.
2. Gan, J.; Zhou, Z.; Yu, A.; Ellis, D.; Attwood, R.; Chen, W. Co-simulation of multibody dynamics and discrete element method for hydraulic excavators. *Powder Technol.* **2023**, *414*, 118001. [CrossRef]
3. Mitrev, R.; Janošević, D.; Marinković, D. Dynamical modelling of hydraulic excavator considered as a multibody system. *Tech. Gaz.* **2017**, *24*, 327–338.
4. Xiang, Q.; Wang, P.; Li, Y. An algorithm of eliminating spike of the measured excavator load spectrum signal based on peak-valley extraction. In *Journal of Physics: Conference Series*; IOP Publishing: Bristol, UK, 2020; Volume 1633, p. 012013.
5. Fragassa, C.; Minak, G.; Pavlovic, A. Measuring deformations in the telescopic boom under static and dynamic load conditions. *Facta Univ. Ser. Mech. Eng.* **2020**, *18*, 315–328. [CrossRef]
6. Wang, P.; Xiang, Q.; Królczyk, G.; Lu, P.; Wang, B.; Li, Z. Dynamic Modeling of a Hydraulic Excavator Stick by Introducing Multi-Case Synthesized Load Spectrum for Bench Fatigue Test. *Machines* **2022**, *10*, 741. [CrossRef]
7. Arsić, D.; Gnjatović, N.; Sedmak, S.; Arsić, A.; Uhričik, M. Integrity assessment and determination of residual fatigue life of vital parts of bucket-wheel excavator operating under dynamic loads. *Eng. Fail. Anal.* **2019**, *105*, 182–195. [CrossRef]
8. Yu, C.; Bao, Y.; Li, Q. Finite element analysis of excavator mechanical behavior and boom structure optimization. *Meas. J. Int. Meas. Confed.* **2021**, *173*, 108637. [CrossRef]
9. Peng, J.; Cheng, X.; Wang, J.; Xiao, L. Contact analysis of heavy-duty apron feeder with clearance. *Eng. Rev.* **2023**, *43*, 91–105. [CrossRef]
10. Edwards, D.; Parn, E.A.; Sing, M.C.P.; Thwala, W.D. Risk of excavators overturning: Determining horizontal centrifugal force when slewing freely suspended loads. *Eng. Constr. Archit. Manag.* **2019**, *26*, 479–498. [CrossRef]
11. Mitrev, R.; Marinković, D. Numerical study of the hydraulic excavator overturning stability during performing lifting operations. *Adv. Mech. Eng.* **2019**, *11*, 1687814019841779. [CrossRef]
12. Jovanovic, V.; Janošević, D.; Marinković, D.; Petrović, N.; Pavlović, J. Railway Load Analysis During the Operation of an Excavator Resting on the Railway Track. *Acta Polytech. Hung.* **2023**, *20*, 79–93. [CrossRef]
13. Yuan, Y.; Ren, J.; Wang, Z.; Mu, X. Dynamic analysis of the rigid-flexible excavator mechanism based on virtual prototype. *Facta Univ. Ser. Mech. Eng.* **2022**, *20*, 341–361. [CrossRef]
14. Liang, G.; Liu, L.; Meng, Y.; Chen, Y.; Bai, G.; Fang, H. Dynamic Modeling and Analysis of Loader Working Mechanism Considering Cooperative Motion with the Vehicle Body. *Machines* **2023**, *11*, 9. [CrossRef]
15. Petrović, G.; Pavlović, J.; Madić, M.; Marinković, D. Optimal Synthesis of Loader Drive Mechanisms: A Group Robust Decision-Making Rule Generation Approach. *Machines* **2022**, *10*, 329. [CrossRef]
16. Lee, J.S.; Ham, Y.; Park, H.; Kim, J. Challenges, tasks, and opportunities in teleoperation of excavator toward human-in-the-loop construction automation. *Autom. Constr.* **2022**, *135*, 104119. [CrossRef]
17. Zhang, L.; Fu, W.; Yuan, X.; Meng, Z. Research on Optimal Control of Excavator Negative Control Swing System. *Processes* **2020**, *8*, 1096. [CrossRef]

18. Cheng, M.; Zhang, J.; Xu, B.; Ding, R. Electrohydraulic Load Sensing System via Compound Control of Flow Feedforward and Pressure Feedback. *J. Mech. Eng.* **2018**, *54*, 262–270. [CrossRef]
19. Qin, T.; Ma, Y.; Li, Y.; Quan, L. Torque equilibrium position closed-loop control of dual electric motors swing system for large mining excavator. *Mechatronics* **2023**, *95*, 103035. [CrossRef]
20. Huang, W.; Zhang, X.; Ge, L.; Quan, L. Dual Source Integrated Driving for Hydraulic Excavator Swing System. *IEEE Access* **2021**, *9*, 120755–120764. [CrossRef]
21. Huang, W.; Quan, L.; Ge, L.; Xia, L. Combined velocity and position control of large inertial hydraulic swing mechanism considering energy balance of supply and demand. *Autom. Constr.* **2019**, *106*, 102899. [CrossRef]
22. Göncz, P.; Drobne, M.; Glodez, S. Computational model for determination of dynamic load capacity of large three-row roller slewing bearings. *Mech. Mach. Theory* **2013**, *32*, 44–53. [CrossRef]
23. Šalinić, S.; Nikolić, M.; Bošković, G. Contribution of the Determination of the Load on Suspension Ring of the Underframe of the Hydraulic Excavator. *IMK-14 Res. Dev. Heavy Mach.* **2014**, *20*, 129–133.
24. Smolnicki, T.; Stańco, M.; Derlukiewicz, D. Distribution of loads in the large size bearing—Problems of identification. *Tech. Gaz.* **2013**, *20*, 831–836.
25. Jovanovic, V.; Marinković, D.; Petrović, N.; Stojanović, D. The Load Spectrum of Axial Bearing of Hydraulics Excavator with Shovel Attachment. *J. Eng. Manag. Syst. Eng.* **2024**, *3*, 175–182. [CrossRef]
26. Xiao, J.; Wu, Y.; Long, W.; Xu, C. Failure Analysis of Gantry Crane Slewing Bearing Based on Gear Position Accuracy Error. *Appl. Sci.* **2022**, *12*, 11907. [CrossRef]
27. Skyba, R.; Hrček, S.; Smetánka, L.; Majchrá, M. Contact pressure analysis of slewing rings. In *IOP Conference Series: Materials Science and Engineering*; IOP Publishing: Bristol, UK, 2019; Volume 659.
28. He, P.; Wang, Y.; Liu, H.; Guo, E.; Wang, H. Influence of the elastic and elastic-plastic material parameters on the mechanical properties of slewing bearings. *Adv. Mech. Eng.* **2021**, *13*, 1687814021992151. [CrossRef]
29. Marek, K.; Piotr, S. The fem application in numerical analysis of slewing rings roller/ball combination bearing. *Commun. Sci. Lett. Univ. Zilina* **2017**, *19*, 3–9. [CrossRef]
30. He, P.; Ding, Y.; Wang, Y.; Li, F.; Liu, W.; Wang, H. A New Analysis Method for the Carrying Capacity of Three-Row Roller Slewing Bearing. *Mechanika* **2022**, *28*, 266–272.
31. Potočnik, R.; Göncz, P.; Glodež, S. Static capacity of a large double row slewing ball bearing with predefined irregular geometry. *Mech. Mach. Theory* **2013**, *64*, 67–79. [CrossRef]
32. Jovanovic, V.; Marinković, D.; Janošević, D.; Petrović, N. Influential Factors in the Loading of the Axial Bearing of the Slewing Platform Drive in Hydraulic Excavators. *Tech. Gaz.* **2023**, *30*, 158–168.
33. Marek, K.; Robert, U. Analysis of the influence of slewing bearing mounting on their static load capacity. *Transp. Res. Procedia* **2019**, *40*, 745–750.
34. Piotr, R.; Kania, L.; Pytlarz, R. Numerical analysis of the screw connection with preload tension used in the mounting of slewing bearings. *J. KONES* **2015**, *19*, 465–472.
35. Mascenik, J.; Coranic, T. Experimental Determination of the Coefficient of Friction on a Screw Joint. *Appl. Sci.* **2022**, *12*, 11987. [CrossRef]
36. Yu, Y.; Do, T.C.; Park, Y.; Ahn, K.K. Energy saving of hybrid hydraulic excavator with innovative powertrain. *Energy Convers. Manag.* **2021**, *244*, 114447. [CrossRef]
37. Rexroth A Bosch Company. Available online: https://www.boschrexroth.com/web/161ed0d4-cb8d-408b-9def-9fd158670577 (accessed on 9 June 2024).
38. CAT Company. Available online: https://www.cat.com/en_US/products/new/equipment/excavators.html (accessed on 15 September 2024).
39. Houman, H. *Hydraulic Formulary*; Rexroth Bosch Group: Lohr am Main, Germany, 2013; pp. 1–43.
40. Kizielewicz, B.; Sałabun, W. SITW Method: A New Approach to Re-identifying Multi-criteria Weights in Complex Decision Analysis. *Spectr. Mech. Eng. Oper. Res.* **2024**, *1*, 215–226. [CrossRef]